Proposed Cortical "Shutter" Mechanism in Cinematographic Perception

Walter J. Freeman

Abstract Brains are open thermodynamic systems, continually dissipating metabolic energy in forming cinematographic spatiotemporal patterns of neural activity. In this report patterns of cortical oscillations are described as 'dissipative structures' formed near an operating point at criticality far from equilibrium. Around that point exists a small-signal, near-linear range in which pairs of impulse responses superpose. Piece-wise linearization extends analysis into nonlinear ranges. Resulting root loci are interpreted as projections from a phase plane, in which the three phase boundaries are graphed in the coordinates of rate of change in a dynamic order parameter (negentropy) on the ordinate analogous to static pressure *vs.* rate of energy dissipation (power) analogous to static temperature on the abscissa. The graph displays the neural mechanism that implements phase transitions and enables the limbic system to repeat the action-perception cycle at 3–7 Hz. The mechanism is null spikes ('vortices') in Rayleigh noise in background electrocorticogram (ECoG) that serve as a shutter by triggering phase transitions.

1 Introduction

Measurements from depth electrodes of microscopic axonal action potentials [1, 2], pial surface electrodes of mesoscopic dendritic potentials giving the electrocorticogram (ECoG [3, 4, 5, 6]), and scalp electrodes giving the macroscopic electroencephalogram (EEG) show that brains, as chaotic systems [7], don't merely *filter* and *process* sensory *information*. Brains import raw sense data that is represented by *microscopic* stimulus-driven spike activity. They replace it by constructing *mesoscopic* percepts that are manifested in spatiotemporal patterns of wave packets [8, 9, 10]. These local patterns combine into *macroscopic* states that involve much or even all of each cerebral hemisphere [11, 12]. They do this several times a second in the sensory system in sequences of wave packets [10, 12] both asynchronously with local time-varying frequencies [13] and globally synchronized at the same frequency [14].

This Chapter draws on diverse experimental evidence to outline a neural mechanism for the repetitive state transitions that initiate construction of cinematographic sequences, for which clinical evidence has been cited [15]. Section 2 describes the

L. I. Perlovsky, R. Kozma, *Neurodynamics of Cognition and Consciousness.*

spatiotemporal patterns of electrocorticograms (ECoG) that are recorded from the olfactory system during arousal and reinforcement learning. The same basic patterns occur in neocortical sensory systems. Section 3 introduces mutual excitation and the positive feedback by which cortical background activity is created and stabilized. Section 4 introduces inhibition and the negative feedback by which the carrier oscillations of wave packets are generated and stabilized. The concept is developed of bistability through input-dependent changes in nonlinear feedback gain that switch sensory cortices between receiving and transmitting states. Section 5 summarizes evidence for conditional stabilization at self-organized criticality, by which state transitions between these two states of cortex can be described as phase transitions in metastability near pseudo-equilibrium. Section 6 derives a diagram of thermodynamic phase space and phase transitions for cortex far from equilibrium that summarizes cortical operations in the action-perception cycle [16]. Section 7 describes the 'shutter', discusses its significance in perception, and summarizes.

2 Evoked *versus* Induced Activity in the Olfactory and Neocortical Sensory Systems

The creative property of nonlinear dynamics is not readily apparent in the homeostatic feedback mechanisms of brain reflexes, which insure the stability of brain function by keeping the internal environment (temperature, pressure, volume, and chemical constitution) of the brain near optimal levels despite environmental vicissitudes. It becomes clear in modeling perception, which requires creative interaction with the external environment for achieving life goals. A relatively simple example comes from study of neural activity in the olfactory bulb. The olfactory system is a semi-autonomous module that interacts with other parts of the forebrain by exchanging neural information. It receives sensory input and also centrifugal controls through release of neuromodulators from brain stem nuclei. An orchestrated mix of neuroamines and neuropeptides [50] modulates the receptivity of the bulb and olfactory cortex in arousal, search, and learning (Fig. 1).

Endogenous oscillatory activity persists after the olfactory system has been surgically isolated from the rest of the brain, which shows that its basic functions are self-organizing. However, its aperiodic chaotic activity disappears when its parts have been surgically disconnected [14], showing that its aperiodic activity is a global property that is not due to the entrainment of single neurons acting as chaotic generators. This is important, because the stimuli that are recognized in perception are spatiotemporal patterns, such as a facial expression, a musical phrase, the fit of a jacket on the torso, etc. The sensory receptor activity they excite or inhibit are characterized by spatial relationships between each part and every other part of a pattern, so that the determinants of perception in sensory cortical function must also be global, not local as in *feature detector* neurons.

Simultaneous recordings of ECoG activity from arrays of 64 electrodes placed on the olfactory bulb and cortex of rabbits demonstrate the spatial coherence of ECoG oscillations carrying spatiotemporal patterns. In every subject the recordings

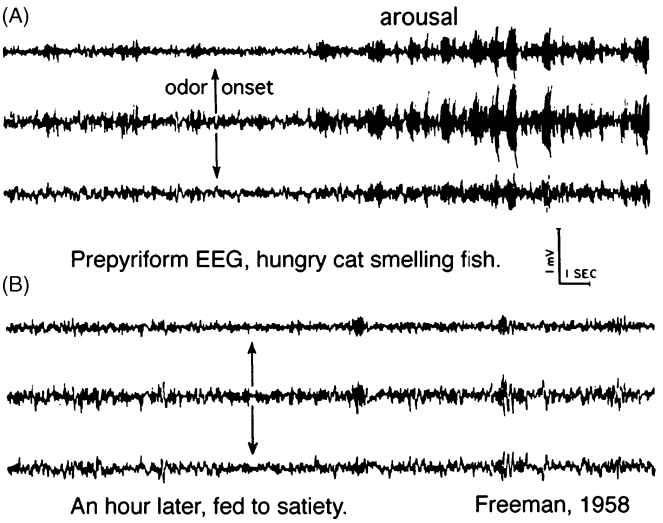

Fig. 1 (**A**) a food-deprived cat at rest is aroused by an odor of fish and searches for it by sniffing, (**B**) after feeding to satiety there is no arousal [14], Fig. 7.17, p. 442

reveal a shared oscillation in cortical potential over the entire array at the same instantaneous frequency [29, 32, 53]. The fluctuation serves as a carrier wave for perception by means of spatial patterns of amplitude modulation (AM) (Fig. 2, left). The spatiotemporal patterns of the frequency of firing of bulbar and cortical neurons are correlated with the AM patterns. The shared carrier waveform is usually aperiodic and unpredictable, reflecting the chaotic dynamics of sensory cortices.

The spatial AM patterns in the sensory cortices cannot literally represent the stimuli that are transmitted to them over their sensory input pathways, because they lack invariance with respect to unchanging stimuli [5, 18, 29, 32, 48, 50, 53, 57]. They change instead with changes in reinforcements, the learning of other new conditioned stimuli (CS) in serial conditioning, and other contextual changes that are associated with stimuli during periods of training to respond to them, in brief, the meanings of the CS, which are as unique for each of the subjects as are the AM patterns. These properties have also been found in ECoG of visual, auditory and somatic neocortices, and they hold in both the beta and gamma ranges. Owing to the fact that the waveform is everywhere similar, the AM pattern of each frame can be represented by a contour plot (Fig. 2, left) of the 64 root mean square amplitudes of the beta (12–30 Hz) or gamma (30–80 Hz) oscillation in each frame. The 64 values specify a vector and a point in 64-space. Similar patterns form clusters of points in 64-space, which can be visualized by use of discriminant analysis to project them into 2-space (Fig. 2, right). In discriminative conditioning with 2 or more CS, the classification of frames is done by calculating the Euclidean distances of the data points from each point/frame to the centers of gravity of the clusters and finding the shortest distance.

When ECoG is observed over time spans of minutes to hours or years, the olfactory dynamic mechanism appears robustly stable in a wide range of amplitudes.

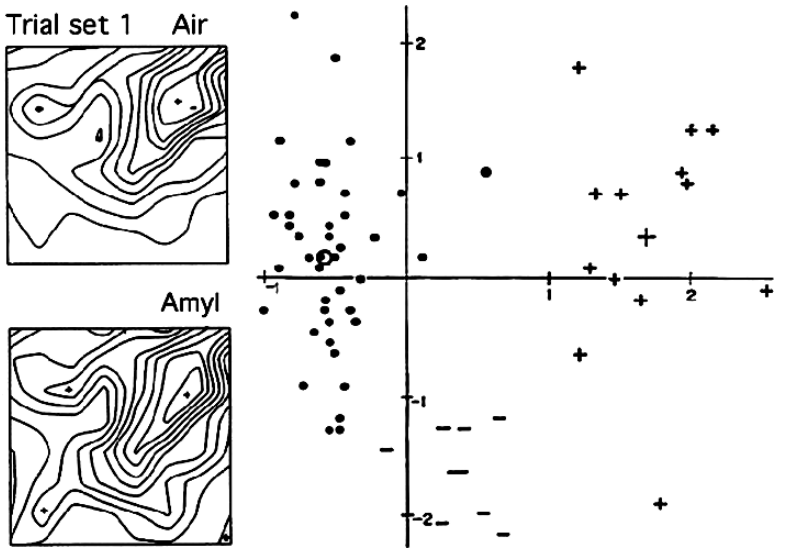

Fig. 2 Left: examples of contours of root mean square amplitude of 64 ECoG segments from and 8×8 (4×4 mm) array on the olfactory bulb. From [32]. **Right**: clusters of points projected from 64-space by discriminant analysis showing classification of patterns by Euclidean distances of points from the three centers of gravity for control (air •), a reinforced odorant (amyl acetate +), and an unreinforced odorant (butyl alcohol -). From [53]

The stability in the olfactory system and in neocortex has been explored in detail in terms of *chaotic attractor landscapes* [42, 57], *metastability* based in "*coordination dynamics*" [11, 40], *chaotic itinerancy* [59], and *explicit vs. spontaneous symmetry breaking* among multiple ground states in dissipative many-body physics [33]. In the course of normal behavior the states are changed by neuromodulatory inputs from the hypothalamus and brain stem that induce transitions such as those between stable states of waking and sleep. Abnormally, the waking state is destabilized by intense excitation leading to transmitter depletion, causing the brain to transit to an alternative state that is characterized by a form of epilepsy [16]: complex partial seizures that include behavioral *absence* (loss of consciousness with failure to attend, perceive or learn). An important normal form of destabilization occurs during learning to identify a new odorant, which requires the actions of neuromodulatory nuclei in the brain stem that release neuroamines and neuropeptides under limbic control.

These properties indicate the need to distinguish among three types of change in both olfactory and neocortical dynamics. First, a physiological stimulus to receptors causes a pattern of action potentials that through relays from receptors injects a pattern of spikes into the bulb that represents the stimulus. The driven cortical response is an evoked potential. By itself the input does not force a state transition, but it perturbs the dynamics and, when ended, allows the system to relax to its prestimulus state without changing the cortical dynamics. Second, learning establishes an attractor landscape in the cortex. Each attractor is surrounded by its basin of attraction that corresponds to the generalization gradient for a category of stimulus

[48]. Formation of a new basin and its attractor is an irreversible structural bifurcation [41, 42]. Third, an act of perception is triggered by the representation of a stimulus when the relevant action potentials select an attractor in the landscape. The percept is dependent on a spatiotemporal activity pattern that is shaped by synaptic weights that e shaped by prior Hebbian and non-Hebbian learning [13]. These modified synapses that store diverse forms of experience form nerve cell assemblies that are intermingled and overlapping. At each moment of engagement by a subject with the environment, a selection must be made in the primary sensory cortices by priming the relevant cell assemblies, that is, by enhancing their excitability and sensitivity to anticipated input. That preparation for selection is done by a process that is called "preafference" [39], Bressler Chapter. This process has been identified with the formation of a global pattern of synchronous oscillation [20, 30, 31] that is established through widespread exchanges of action potentials among sensory cortices and the limbic system. The global pattern elicits and modulates the attractor landscapes of all sensory cortices simultaneously, thereby preparing them for the range of expected outcomes following each act of observation on the environment.

This global state of preparedness in anticipation constitutes a metastable state [Kelso Chapter]. The incoming sensory stimuli select one basin of attraction from the landscape in each sensory cortex. This exclusive choice can be referred to as spontaneous symmetry breaking, as distinct from the explicit symmetry breaking of the evoked potential [33]. The transition from high-dimensional chaos to more stable dynamics with the selection of a lower-dimensional attractor may correspond to dynamic logic [Perlovsky Chapter], which describes transitions from vague and uncertain potential states not yet realized to a crisp and certain perception and cognition following detection of an anticipated stimulus, as an essential mechanism preceding higher cognitive functions.

The endogenous state transition in the formation of a wave packet having an AM pattern is the essence of an act of perception. Transmission of the AM pattern must be followed by another state transition that returns the cortex to the receiving state. The key evidence for the first transition is provided by measurements of the pattern of phase modulation of the beta or gamma carrier waves of successive bursts. Each AM pattern is accompanied by a spatiotemporal pattern of phase modulation (PM). The phase is defined at the dominant or mean carrier frequency in the immediate past. The onset of the transition is characterized by an apparent discontinuity in the phase resembling "phase slip", followed by emergence of a new carrier frequency, on average differing by $\pm$10–20 Hz. The spatial pattern of the phase has the form of a cone (Fig. 3, left) for which the apex is either maximal lead or maxmimal lag. The cone is displayed by concentric circles representing isophase contours. The cone appears because a state transition in a distributed medium does not occur everywhere instantaneously. Like the formation of a snowflake or raindrop it begins at a site of nucleation and spreads radially. The phase gradient in rad/m divided by the carrier frequency in rad/s gives the phase velocity in m/s. The observed phase velocities conform to the conduction velocities of propagated action potentials on axons running parallel to the cortical surfaces. The apical location and sign vary randomly between successive frames (Fig. 3, right). The spread depends on the existence of a small proportion of long axons among the predominantly short axons [42]. The sign

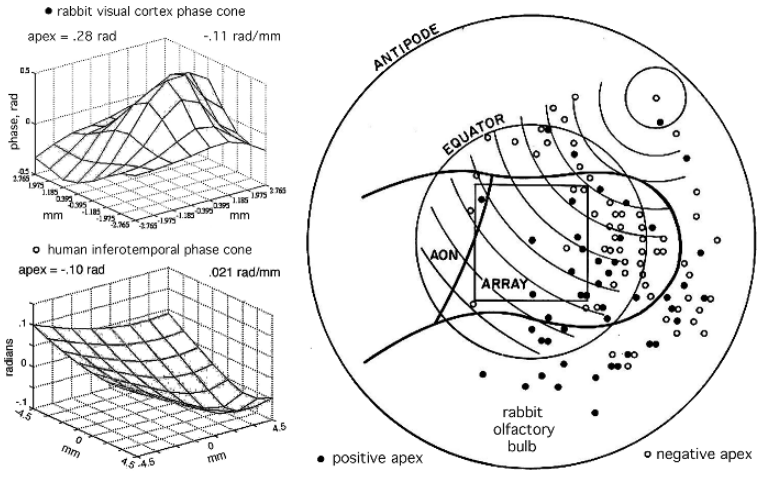

Fig. 3 Left: examples of phase cones from neocortical ECoG of human and rabbit. From [30]. **Right**: outline of rabbit bulb with square array superimposed on the opened spherical surface. The arcs show a representative phase cone; the dark symbols ● show the locations of positive apices ("*explosion*"); the light symbols ^{o} show negative apices ("*implosion*"). From [24]

at the apex depends on whether the short axons (phase lead at the apex, explosion) or the long axons (phase lag at the apex, implosion) dominate the transmission.

These properties show that the state transition is an endogenous property of distributed cortical networks. It cannot be attributed to a localized "pacemaker" in the cortex, thalamus, or striatum. Then there is the second state transition that returns the cortex to the receiving state is intrinsic to the cortical background activity. There is no apparent phase discontinuity. Instead, the analytic amplitude may diminish to such a low level that the phase becomes undefined. If in this condition there is fresh input to the cortex, the possibility emerges of a new state transition. Recurrence of the episodic phase re-setting gives the cinematographic sequences of wave packets expressed in AM and PM frames. Each frame begins after the phase discontinuity manifests phase re-setting. The time lapse before the cone disappears demonstrates the duration of the frame.

Next the question is addressed, to what extent might the dynamics of the olfactory system hold for other sensory areas? The main components of the olfactory system are allocortex. This is an ancient three-layered neuropil that is found in all vertebrates in a variety of forms. The six-layered neocortex, found only in mammals, is far more complex and has widely varying forms and degrees of specialization. The relative simplicity of allocortical structure and dynamics makes it a good platform from which to discern what properties might be fundamental in the dynamics of neocortex. The visual, auditory and somatic sensory cortices, all or which are neocortical, reveal the same basic modes of operation in perception as in olfaction: the genesis of broad-spectrum, aperiodic ECoG activity with statistically correlated spike activity; formation of successive wave packets with spatially coherent carrier waves; AM patterns that are classifiable with respect to learned conditioned stimuli and responses (CS and CR); and accompanying PM patterns in the form of a cone

(Fig. 3, left) with randomly varying location and sign of the apices. Neocortical AM and PM patterns are larger and more complex than allocortical patterns, and they lack the easy frame marker provided by respiration and sniffing (the bursts of gamma seen in Fig. 1, A). Otherwise the properties described in this and the following sections hold for both types of cortex. Paramount among these properties is the ubiquitous background activity, which holds the key to understanding cortical function and therefore higher cognitive function.

3 Self-organization by Positive Feedback: Mutual Excitation and Excitatory Bias

The pervasive *spontaneous* activity of cerebral cortex is easily observed both in spikes from axons and in field potentials from dendritic current seen in ECoG (Fig. 1). The source of this activity has been identified as mutual excitation among excitatory cells [14, 22]. In neocortex 80% of the neurons are pyramidal cells, which are excitatory, and 90% of their synapses are from intracortical neurons. The 10% of synapses from sources outside cortex are excitatory. Therefore, the overwhelming interaction among neocortical neurons is by mutual excitation among pyramidal cells. In the olfactory bulb the organization differs, because the equivalents of pyramidal cells (the mitral and tufted cells) are outnumbered >100:1 by the equivalent inhibitory interneurons (the internal granule cells). A dynamic balance is maintained by a large population of excitatory interneurons (the periglomerular cells in the outer layer bulb) [14]. These neurons transmit and receive by GABA, so they are commonly misidentified as inhibitory interneurons; however, their high content of chloride ions [56] makes their GABA-A synapses excitatory. Their sustained mutually excitatory activity is not the same as that of the "reverberatory circuits" of Hebb and Lashley for putative temporary storage of memories [2] in small nerve cell assemblies [49]. Instead their background activity is steady state and large scale.

The mechanism in periglomerular and other excitatory populations has been described using a network of ordinary differential equations (ODE) [14]. The topology of connections in neural populations is represented (Fig. 4) by K-sets of neurons of like kind. The simplest are populations of noninteractive neurons of two kinds: KOe excitatory or KOi inhibitory, which when synchronously activated behave as would an average neuron, but with state variables of wave and pulse densities in place of membrane currents and spike trains. A KIe population of interacting excitatory neurons such as the periglomerular cells can, by consideration of symmetry conditions, be reduced to a positive feedback loop, in which the dynamics of the KOe forward and feedback limbs is identical, because each neuron in the receiving state continually renews the population in the transmitting state. Each limb is described by weighted linear summation of wave density in dendrites and static nonlinear conversion of wave density to pulse density. The dendritic operation can be described by a 2^{nd} order linear ODE with gain constants for the synapses. The solution of the ODE for impulse input conforms to the dendritic postsynaptic potential (PSP)

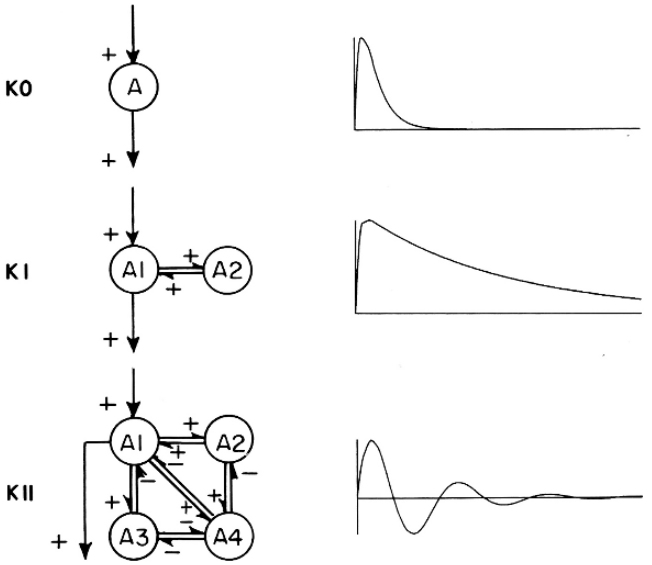

Fig. 4 KO represents the dynamics of a non-interactive population; the response to impulse input (single shock electrical stimulation) corresponds to the postsynaptic dendritic potential of single neurons. KI represents an interactive population of like kind: excitatory KIe or inhibitory KIi with a prolonged monotonic closed loop impulse response (averaged evoked potential AEP and PSTH). KII represents interaction between excitatory KIe and inhibitory KIi neuron populations with an oscillatory closed loop impulse response (AEP or PSTH). From [14], Fig. 1.6, p. 40

of single neurons to single-shock impulse input: a rapid exponential rise governed by synaptic delay and the cable properties of the dendrites, followed by exponential decay that is governed by passive membrane resistance and capacitance (Fig. 4, KO). In a population of neurons the output of the axons is observed in a post-stimulus time histogram (PSTH) of representative single neurons that has the same form and rate constants as the summed PSP of the dendrites.

Conversion from dendritic wave density to axonal pulse density at trigger zones is governed by an asymmetric sigmoid function [14, 15] (Fig. 5). The nonlinear thresholds of the axons determine lower asymptote. The neurons cannot fire when they are inhibited below threshold by input from inhibitory interneurons. The upper asymptote is determined by the axon refractory periods. The neurons cannot fire with excitatory input when they have already recently fired.

Piecewise linearization [14] of cortical dynamics is achieved by replacing the nonlinear function (Fig. 5) with a constant gain value given by the slope of the tangent to the sigmoid curve at a specified operating point for wave density input and pulse density output. The operating point in the steady state is at unity gain, when input amplitude is equal to output amplitude. The displacement from a steady state set point by impulse or sustained input can raise or lower the gain from unity. There are two stable set points at unity gain: one is found in the KIe set at normalized wave density $v > 0$ (Fig. 5, A). The other set point is found at $v = 0$ in the KII set, which is formed by the interaction between a KIe set and a KIi set. The mutually

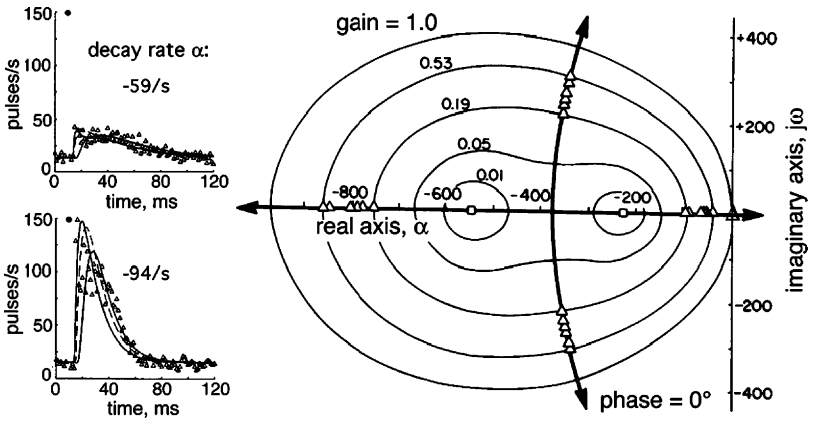

Fig. 5 Wave-to-pulse conversion at trigger zones in populations is governed by a static nonlinearity, which is the asymmetric sigmoid curve that is shown with a high slope in arousal (Fig. 1, A) and a low slope in rest (Fig. 1, B). The pairs of curves asymptotic to zero show the derivative of the sigmoid curve, which gives the nonlinear gain. Linear approximation is by replacing the function with the tangent at the desired operating point, for which the slope approximates the fixed feedback gain. A : KIe set, B: KIIob set. Equations are given in [1, 14, 49]

inhibitory KIi set has a stable set point only at zero gain giving a flat ECoG, so a KIi set is nonfunctional without an excitatory bias from one or more KIe sets. The maximal asymptote, Q_m, is determined by refractory periods; however, as indicated by Fig. 5, Q_m varies with the level of arousal under limbic control. Two levels are shown in Fig. 5. The ECoG with arousal state is seen in Fig. 1, A. The ECoG in the rest state is seen in Fig. 1, B.

The impulse response of the closed loop KIe system (Fig. 1, KI) is given by the averaged, single-shock evoked potential (AEP) in the wave density mode (ECoG recording) or by the post-stimulus time histogram (PSTH) in the pulse density mode (time-locked averages of spike train recording from single neurons, Fig. 6, left, or multiunit recording – not shown). The utility of the impulse response lies in the information it gives about the state of the system and its dynamic properties, because it contains all frequencies, and so it reveals the characteristic frequencies of the neural population in its current near-linear operating state. These properties are displayed in a state space diagram (Fig. 6, right) that is derived by linearization of the two coupled 2nd-order nonlinear ODE that model KIe dynamics in the vicinity of the prestimulus operating point (Fig. 5, A). Averaging of the impulse responses (Fig. 6, left) from repeated stimulation at regular time intervals is necessary to remove the microscopic background activity treated as *noise* and extract the mesoscopic *signal*, which is the trajectory by which the system returns to its prestimulus state after each impulse.

Linear analysis is the most powerful tool available to neurodynamicists [6, 7, 12, 34, 44, 63]. In the variant using root locus analysis the characteristic frequencies of the linearized system are represented as closed loop poles (small triangles Δ in Fig. 6, right), and the characteristic forbidden "anti-resonant" frequencies are shown as zeroes ((unknown char) in Fig. 6, right) in the roots of 2 coupled

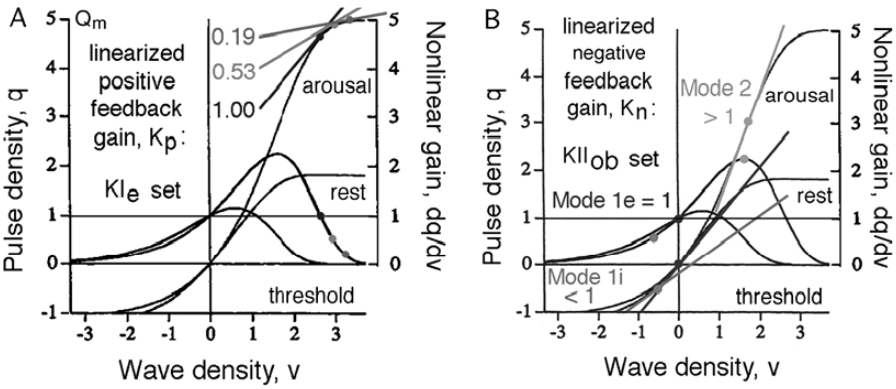

Fig. 6 Left: Impulse responses of a periglomerular cell on excitation of the primary olfactory nerve at 6 intensities. Data (Δ) in averaged post-stimulus time histograms were fitted with solutions to a matrix of four 1st order ODE. **Right**: Root loci (*dark lines*) of the changes in poles as a function of gain (elliptical contours), k_p. At zero gain the poles (Δ) lie at the open loop values (⊓), rise rate = -530/s, decay rate = -230.sl . The left-right arrows indicate the direction of change in the real rate constants as gain contours (*ellipses*) increase to infinity. The up-down arrows show the direction of approach of the complex conjugate roots to zeroes in the right half of the complex plane (not shown). From [14], Fig. 5.10 p. 289, Fig. 5.13 p. 292

2nd-order ODE representing the closed loop dynamics. The open loop poles in the feedback ODE become the zeroes in the closed loop, small-signal, linearized 4th- order transfer function (the symbols (unknown char) on the left half of the negative real axis in Fig. 6, right).

A very useful experimental control parameter is the intensity of the impulse (the product of amplitude and duration). Changing the stimulus intensity causes the characteristic frequencies in the response to change. The changes in frequency are translated graphically into the most useful physiological parameters, which is the strengths of interaction (gains) between populations of neurons. The frequencies (roots) change along the heavy lines (root loci), and the gains are calculated as the values for linearized closed loop gain (the intersections of the root loci with the contours in Fig. 6, right). When the intensity is raised or lowered, the characteristic frequencies of the open loop components of the system (the synapses and their strengths) are not changed, but the functional properties of the system are altered by the amplitude-dependent nonlinearity at the trigger zones that is described by the asymmetric sigmoid curve (Fig. 5, A). Changing the response amplitudes by changing the input intensity changes the characteristic frequencies of the closed loop poles and zeroes by changing the set points at which the tangent slope is calculated. With systematic step-wise change in stimulus intensity, the changed values of the closed loop poles inscribe the root loci (orthogonal to the gain contours).

These root loci (at zero radians phase in positive feedback and at p radians phase in negative feedback) quantify the degree of stability of the system and specify how a change in the input can bring about either greater stability with resistance to state transition (poles moving to the left away from the imaginary axis), or to lesser stability and an increase in likelihood of a transition to a new state (poles

moving to the right toward the imaginary axis). The postulate to be considered is that the formation of an AM pattern during an act of perception might take place when poles shift to the right of the imaginary axis, giving exponential terms with positive rates of increase.

The arrowheads on the root loci in Fig. 6 indicate the direction in which gain increases with decreasing response amplitude. On the one hand, strong impulse that drives an increase in impulse intensity increases response amplitude and decreases feedback gain, which increases the decay rate to the prestimulus background level. The decrease in KIe feedback gain with increased input intensity is due to the refractory periods; neurons that are challenged to fire cannot do so if they have recently already fired. On the other hand, extrapolation of the decay rate of the PSTH to zero input (response threshold) gives zero decay rate. Such a response would be a step function [14]); it cannot be observed, because it has zero amplitude. The extrapolation of the decay rates to zero and the feedback gain to unity at threshold using this root locus demonstrates that the population is self-stabilized at its steady state excitatory output by refractory periods without need for inhibition. The pole at the origin of the complex plane (Fig. 6, right, large Δ) conforms to a zero eigenvalue (zero rate of change, an infinite time constant).

That pole represents the functional steady state of the KIe population that would hold in the absence of input: steady state excitatory pulse density output, the background activity. The state is stable, because excitatory input raises the output but decreases the gain, so the population activity tends toward the steady state level. Decreased excitatory input or increased inhibitory input does the reverse. Therefore the pole represents a point attractor, which differs from the state of zero activity under deep anesthesia or in death, in that the mutual excitation provides sustained, stable, steady state excitatory bias within itself and to other neural populations in the olfactory system. The non-zero point attractor governs the KIe population dynamics and modulates all other populations that receive the excitatory bias.

Direct experimental observation of the pole at the origin is obviously not possible, because the impulse response has zero amplitude and zero decay rate. Moreover, every KIe population has on-going input from other populations, including the periglomerular population getting both sensory input and centrifugal input from other parts of the forebrain, so the observed steady state gives a pole that is displaced to the negative side of zero frequency on the real axis of the complex plane (gain = 0.53).

The root locus method requires piecewise linearization of the dynamics. The technique depends on the fact that the impulse input does not change the system structure. Instead the input imposes an extra term, a perturbation superimposed on the background activity that reveals the dynamics by the trajectory of relaxation back to the prestimulus state: the *explicit breakdown of symmetry*, in contrast to the *spontaneous breakdown of symmetry* [33] that, as will be shown, characterizes perception. The same pair of 2nd-order ODE is applicable across the whole range of piecewise linearization but with a different value of the gain parameter for each level of input. More generally, populations of neurons that share the properties of thresholds, refractory periods, and mutual excitation can be described as governed by a non-zero point attractor, which describes the process by which excitatory

populations maintain non-zero steady state background activity without need for inhibition to prevent runaway excitatory discharge. Thereby mutual excitation provides the excitatory bias in cortex that is essential for maintaining "spontaneous" background activity. This activity in many circumstances has been shown to have approximately a Gaussian noise amplitude histogram and a power-law power spectral density with slope near -2 ($1/f^2$, "brown noise" [55]).

4 Measuring and Modeling Oscillations Using Root Loci in Piecewise Linearization

The introduction of inhibitory neurons (Fig. 4, KII) is required not for stabilization of neural networks but for oscillations, most notably in the olfactory system for oscillations in the gamma range, 30–80 Hz (Fig. 1, A and Fig. 4 KII, Fig. 7, left). The specification of a central frequency in this range, 40 Hz, is immediately apparent from measurement of the open loop time constants (Fig. 4 KO) of the PSP or PSTH, the impulse responses of the non-interactive excitatory and inhibitory neurons comprising the olfactory populations. The exponential rise times average near 1.25 ms; the exponential decay times are near 5 ms. One cycle of oscillation requires two passages around the loop, giving a total delay of 25 ms (the wave

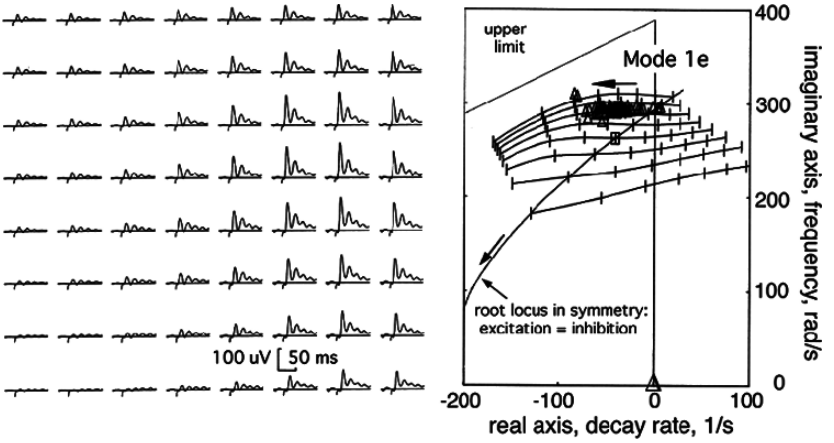

Fig. 7 Left: A set of 64 simultaneously derived impulse responses from an 8×8 4×4 mm array of electrodes for recording ECoG (the square frames in Fig. 3 left and the open square inset in Fig. 2, right) gave different amplitudes at different locations on single-shock stimulation of the olfactory nerve. The upward shift in baseline was provided by the KIe periglomerular neurons with positive gain k_p (shown by the PSTH in Fig. 6, left). Oscillations all had the same frequency, with decay rates proportional to amplitude. From [14], Fig. 4.27 p. 221. **Right**: the poles given by the frequencies and decay rates of the dominant damped cosine wave that was fitted to each of the 64 impulse responses gave root locus Mode 1e for the KII set with maintenance of unity gain (Fig. 5, B). The leftward arrows indicate the increased decay rate of the evoked gamma oscillation at sites with increased response amplitude due to gain reduction by refractory periods. From [14], Fig. 6.86 p. 361

duration of 40 Hz). However, the excitatory neurons excite each other, and the inhibitory neurons inhibit each other, as well as interacting in negative feedback (Fig. 1, KII). These two types of positive feedback — mutual excitation in the KIe population and mutual inhibition in the KIi population — modulate the frequency of negative feedback over the gamma range by variation in the 4 types of forward gain: excitatory or inhibitory synapses on excitatory or inhibitory neurons. If the four gains are set equal and changed concurrently, the symmetry of mutual excitation and mutual inhibition results in pole-zero cancellation. The root locus (phase = p radians in negative feedback) is shown for the upper half of the complex plane as the arc ("symmetry" in Fig. 7, right) rising with increasing negative feedback gain from the open loop pole (shown on Fig. 6 at a = –230/s) on the negative real axis and crossing the imaginary axis near 300 rad/s (50 Hz). The centered small rectangle (unknown char) identifies the average state or rest point that is observed for impulse responses at near-threshold impulse input by single-shock stimulation of the primary olfactory nerve [14]. This route of input to the bulb is called "orthodromic" because the direction of transmission conforms to the normal input of action potentials to the bulb from the sensory receptors in the nose. In contrast, electric excitation of the output path of the bulb, the lateral olfactory tract formed by axons of mitral cells, is called "antidromic", because the evoked action potentials travel into the bulb abnormally, that is, in the opposite direction to normal propagation (Fig. 8).

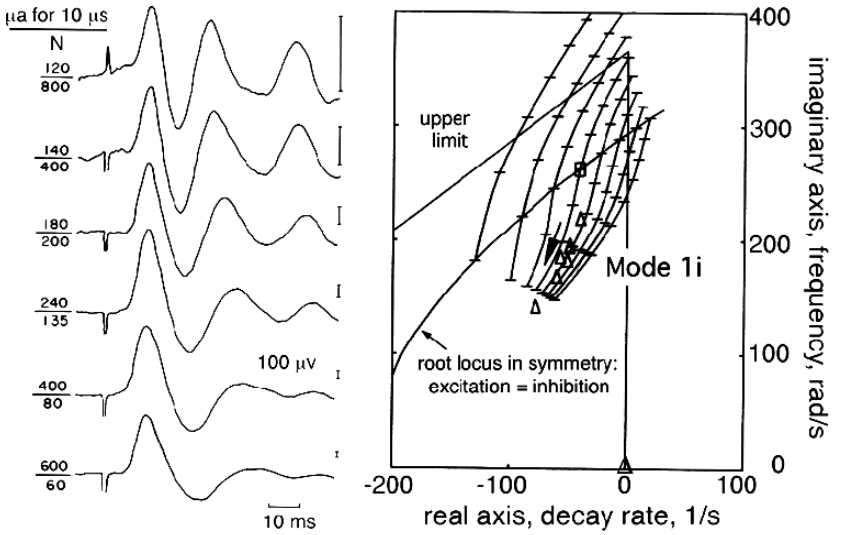

Fig. 8 Left: antidromic single-shocks to the lateral olfactory tract evoked impulse responses in the bulb, which bypassed the periglomerular neurons and the excitatory bias they contributed to the input. With increasing stimulus intensity the frequency decreased with little change in decay rate, giving a vertical root locus. **Right**: root loci from solving ODE for impulse responses predicting frequencies and decay rates. The same Mode 1i root loci are derived from impulse responses obtained with fixed impulse intensity while reducing the background activity by administration of barbiturate anesthesia. That is, the frequency of oscillation is determined by the ratio of evoked activity to background activity, when the evoked potential exceeds the background. From [14], Fig. 6.11, p. 374

Mode 1e shows the increased stability imposed by the bulbar mechanism in response to irrelevant or noisy input. The upper line shows the limit imposed by the value of the feedback gain in the KIe population that gives a pole at the origin of the complex plane for unity positive feedback gain, $k_p = 1$. That is, when the bombarding input to cortex abates, the cortex can settle toward its internal steady state amplitude of background activity governed by the non-zero attractor represented by the pole at the origin of the complex plane. Then the oscillatory pole tends toward a higher frequency and faster envelope of decay of the impulse response, but only to the limit of the diagonal line shown as the "upper limit" in the steady state. As with the pole at the origin, oscillator y impulse responses at the limit are not observable.

The impulse responses of the olfactory system (the averaged evoked potentials AEP) for which the peak amplitudes do not exceed the amplitude range of the ongoing background ECoG conform to additivity and proportionality on paired-shock testing, showing that there is a small-signal near-linear range in the dynamics of the major components of the central olfactory system. The arrow downward to the left in Fig. 7 shows the reduction in frequency and increase in decay rate when all feedback gains are reduced equally ("symmetry") by increased input intensity or by reduction of the background bias from KIe sets.

This symmetric root locus under the condition of equality of excitatory and inhibitory positive feedback is rarely seen in experimental root loci derived from evoked potentials, because the mutual excitation (KIe) and mutual inhibition (KIi) are rarely equal. When mutual excitation predominates, the root locus is horizontal (Mode 1e). Stimulation of the input tract to the bulb evokes potentials in which the decay rate is proportional to response amplitude over the spatial distribution of input but the frequency is constant (the horizontal root loci in Fig. 7, right). When mutual inhibition dominates, the root locus can approach vertical (Mode 1i. Fig. 8, right). Antidromic stimulation of the output tract of the bulb, the lateral olfactory tract, activates the inhibitory interneurons directly by dendrodendritic synapses, giving a strong inhibitory bias to the oscillations (Fig. 8, Mode 1i) that is not compensated by KIe input as it is in orthodromic input (Fig. 7, left), because the periglomerular cells are not activated by antidromic stimulation.

Mode 1e and 1i root loci are seen only when the amplitude of the single-shock evoked potentials exceeds the range of the background ECoG amplitudes. This is because the thresholds of the axons during recurrent inhibition limit the amplitude of the evoked activity that exceeds the spontaneous range. When neurons are inhibited below their thresholds, they cannot fire to signal the magnitude of inhibitory input. The thresholds block axonal output that signals excess dendritic inhibition; the block effectively reduces the feedback gain in the KII loop [14], Fig. 5.28, p. 335. In contrast, the refractory periods (not the thresholds) of the axons limit the upper range of background activity and the superimposed evoked potentials (Fig. 5, $k_n > 1$).

When the input intensity is fixed to give evoked potentials for which the peak-to-peak amplitudes do not exceed the range of background activity, the frequency and decay rate of successive averaged evoked potentials are high with low amplitude and high with high amplitude (downward-right arrow, Fig. 9). The variations provide evidence for spontaneous fluctuations in feedback gain and set point,

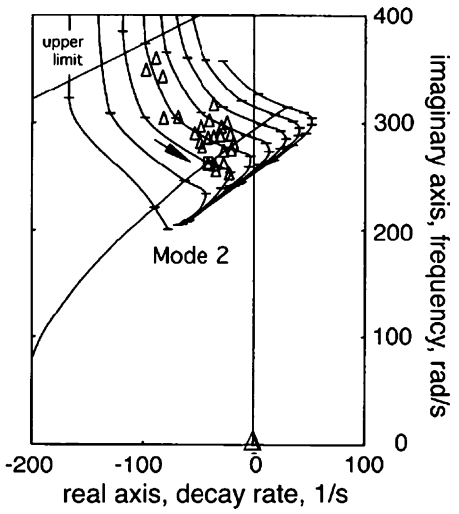

Fig. 9 Closed loop root loci in the upper half of the complex plane at p radians are revealed by the spontaneous variation of the oscillatory impulse responses in the small signal, near-linear range. The small triangles show the characteristic frequencies of the evoked potentials fitted with damped cosines. The arrow shows the direction of decreased decay rate and frequency with increased response amplitude (the reverse direction compared with Mode 1e in Fig. 7, right). From [14], Fig. 6.21, p. 374

owing to spontaneous fluctuations in the levels of the background activity. These relations differ markedly from those of Mode 1e and Mode 1i. Mode 2 root loci from solving the ODE to fit the data (Δ) cross the imaginary axis with increasing amplitude, which implies runaway excitation by positive feedback between amplitude and gain. However, the root loci turn back toward the imaginary axis and converge to a crossing point close to 250 radians/s (40 Hz). That convergence to a complex conjugate pair of poles on the imaginary axis predicts the existence of a limit cycle attractor for the KII set in the middle of the gamma range. The state is predicted to be stable, because further increase in amplitude is prevented by decreased feedback gain. In piecewise linear analysis of observations based on time averages that flatten the background activity (AEP and PSTH) this result predicts bistability: convergence of cortex either to a point attractor or a limit cycle attractor.

5 Definition of a Cortical Order Parameter Related to Information Content of Cortical Activity

The carrier frequency is everywhere the same across the olfactory bulb and likewise across each sensory neocortex, but it tends to vary in time. Owing to this frequency modulation (FM) the study of spatial patterns is optimally done using the instantaneous frequency derived from the Hilbert transform [20, 21, 39], which gives better temporal resolution of AM and PM patterns than does decomposition using the Fourier transform [20, 21]. The digitized values of 64 ECoG from an 8×8 array yield the conic PM pattern of phase modulation (PM) at the instantaneous frequency (Fig. 3, left), for which the isophase contours form equidistant circles around an

apex (Fig. 3, right). This phenomenon is also found in all areas of sensory neocortex, which implies that communication within cortex is with a finite velocity across its surface that is imposed by the necessity for action potentials acting at synapses to provide for phase locking of oscillations at the time-varying carrier frequency. Any form of time averaging across multiple measurements of phase differences between two points must converge to zero phase lag [28] no matter how great the distance between the points.

The analytic amplitude, $A_j(t)$, at the j-th electrode of the 64 electrodes in the array co-varies widely with time. The variation is reflected in the spatial average, $\underline{A}(t)$ (red/grey curve in Fig. 10, A). When $\underline{A}(t)$ approaches zero, the phase becomes undefined. At each spatial location the rate of increase in phase (the instantaneous frequency) transits to a new value that is shared by waves in all other locations, independently of response amplitude. The spatially coherent oscillation re-synchronizes near a new average frequency, typically differing by $\pm$ 10–20 Hz from the average frequency in the prior frame. During the transition the spatial standard deviation of phase differences, $SD_X(t)$, fluctuates around high values (blue/grey curve in Fig. 10, A). There are two reasons. One reason is that at very low analytic amplitudes, the errors of measurement of phase are very large when the phase is indeterminate. The other reason is that the transition is not simultaneous but dispersed in accord with the phase cone but within the range $\pm$ p/4 ($\pm 45^\circ$), the half-power value. Therefore the peaks $SD_X(t)$ provide a marker in the ECoG for locating widely synchronized jumps signifying distributed state transitions in the cortex.

This pattern of inverse relation between $SD_X(t)$ and $\underline{A}(t)$ occurs both in aroused subjects actively engaged in perception [5, 18, 20, 21, 29, 48] and in subjects at rest (Fig. 10, A). The pattern is simulated in a simple way [22]. The transfer function in the positive feedback loop modeling the dynamics of the KIe set can be approximated by a transcendental exponential term having the same form as a 1-D diffusion process. The autocorrelation, cross correlation and interval histograms conform to those of a Poisson process with refractory periods. The pulse trains of the component neurons can be modeled with random numbers. The sum of a large number

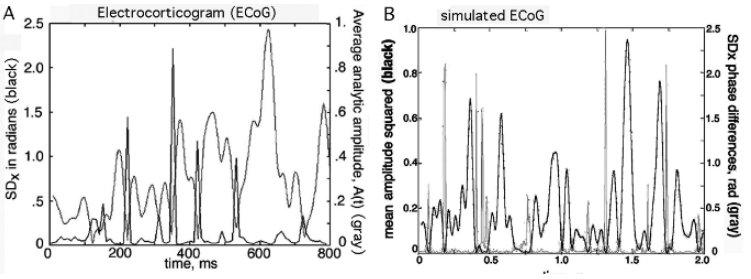

Fig. 10 (**A**) this is an example of ECoG from a human subject at rest, showing the background activity. When the spatial standard deviation of phase differences, $SD_X(t)$, falls to a low value, the mean analytic amplitude, $\underline{A}(t)$, increases to a maximum during the period of relatively constant frequency that follows a state transition [21]. (**B**) this pattern is simulated by passing brown noise $1/f^2$ through a band pass filter in the gamma range. Mean analytic amplitude and spatial variance of analytic phase co-vary inversely [22]

of identical, independently distributed random numbers converges to a power density spectrum with $1/f^2$ slope in log-log coordinates [55]. When this *brown noise* is passed through a band pass filter in the gamma range, the amplitude and phase vary in the manner shown in Fig. 10, B. The cortex provides the pass band at the characteristic frequency the negative feedback relation between the pyramidal (or mitral) cells and the inhibitory interneurons (or internal granule cells) (Fig. 7, right). The result is seen in the fluctuations of the gamma band activity in the ECoG; the amplitude histogram is close to Gaussian; the envelope of the activity conforms to the Rayleigh distribution [14], p. 148, Fig. 3.13c; and the power spectral density in log-log coordinates has a slope near –2. The spikes in $SD_X(t)$ recur erratically in the theta range, as revealed by correlation of ECoG with $SD_X(t)$ in both the real ECoG [20, 21, 26] and the simulation [22]. Therefore the spikes in $SD_X(t)$ in Fig. 10, A can be viewed as intrinsic to the cortical dynamics. The brown noise is generated by KIe dynamics (Figs. 4 and 6); the null spikes emerge when the noise is passed through the KII band pass filter (Fig. 4 and 7). The null spikes are not imposed by the sensory input; instead they reveal episodic intrinsic silencing of the background activity. That momentary silencing may enable perception for the following reason. The cortex passes undergoes a state transition only in the presence of suprathreshold sensory input. The threshold is materially reduced for stimuli for which a Hebbian assembly already exists with its attendant attractor and basin of attraction. The threshold may be still further reduced by the brief abatement in cortical background noise.

The analytic amplitude, $A_j(t)$, also varies with spatial recording location, giving the spatial AM pattern that is represented by a 64×1 vector, $\mathbf{A}(t)$. The vector is normalized by dividing each value of A_j (t) by the mean amplitude, $\underline{A}(t)$. While the AM pattern at every digitizing step is accompanied by a PM pattern, only the patterns that last 3 to 5 cycles of the sustained mean frequency and its phase cone are readily identified, measured, and classified with respect to stimulus categories. The AM patterns with classification of greatest statistical significance are those at the peak of $\underline{A}(t)$, when the rate of increase in the analytic phase (the instantaneous frequency) is nearly constant and the spatial variance in phase, $SD_X(t)$, is low. These are the AM patterns that are classifiable with respect to the CS given to subjects in whom the ECoG is being recorded (Fig. 2, right).

The normalized vector, $\mathbf{A}(t)$, representing AM patterns is adopted as the order parameter for cortex, because it measures the kind and degree of structure in the cortical activity. However, for descriptive purposes a scalar index is needed to show relations of the order parameter to other variables, in particular to the ECoG amplitude. The index is derived as follows. The normalized $\mathbf{A}(t)$ specifies a point in 64-space that represents the AM pattern. Similar patterns form a cluster of points that manifest an attractor in cortical state space. Multiple clusters reveal an attractor landscape. The change from one basin of attraction to another across a boundary (separatrix) is shown by a trajectory of successive digitized points for $\mathbf{A}(t)$, as cortical state shifts from one cluster to another cluster. The absolute rate of change in the order parameter, $D_e(t) = |\mathbf{A}(t) - \mathbf{A}(t\text{-}1)|$, is given by the Euclidean distance between successive points. $D_e(t)$ corresponds to the absolute value of the numerical derivative of the order parameter. It has high values during state transitions and decreases

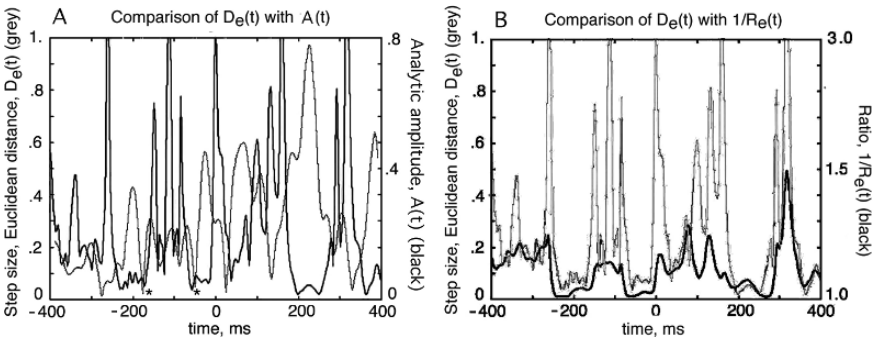

Fig. 11 (**A**): The rate of change in the order parameter, $D_e(t)$, falls to a low value well before a major increase in average analytic amplitude, $\underline{A}(t)$. (**B**): the index of synchrony, $R_e(t)$, (shown here as its reciprocal, $1/R_e(t)$) rises to near unity before the AM patterns stabilize (low $D_e(t)$) and well before $\underline{A}(t)$ increases, showing that increased synchrony is not the basis for increased analytic amplitude in frames of ECoG. From [20]

to low values when a new AM pattern emerges with convergence to an attractor, followed by a major increase in $\underline{\mathbf{A}}$(t) (Fig. 11, A). Therefore D_e(t) varies inversely with the degree of stability of the pattern specified by the vectorial order parameter [20] The degree of order also varies in proportion to the rate of free energy dissipated in cortical activity, which is manifested in the square of the mean ECoG analytic amplitude, $\underline{A}^2$(t). The best available index for locating in time the classifiable AM patterns in the ECoG [18] is the ratio, $H_e(t) = \underline{A}^2(t) / D_e(t)$. Atmanspacher and Scheingraber [3] define this quantity as the *pragmatic information* carried by the wave packet in the beta or gamma range. It is the ratio of the rate of dissipation of free energy to the rate of increase in the order parameter. H_e(t) also provides a unique scalar value to index each classifiable AM pattern as an inequivalent ground state [33].

Desynchronization is commonly associated with low-voltage fast activity, while synchronization is associated with high-voltage slow activity. An increase in mean ECoG analytic amplitude might occur with more synchrony, more total dendritic current, or both. The two factors are distinguished in beta-gamma ECoG records recorded with a high-density 8×8 array by calculating the temporal standard deviation, SD_T(t), of the average waveform in a moving window twice the duration of the wavelength of the center frequency of the pass band and dividing it by the average of the 64 $\underline{SD}_T$(t). When there is no synchrony, the ratio, $R_e(t) = SD_T(t) / \underline{SD}_T(x)$, approaches $1/n^{.5}$, where n is the number of time steps in the window. R_e(t) equals unity when there is complete synchrony (identical instantaneous frequency and phase), whether or not there are AM patterns. R_e(t) is used to show that the major increases in $\underline{A}$(t) during AM pattern formation are not attributable to increases in the level of synchrony (Fig. 11, B), which occur before amplitude increases.

Every classifiable AM pattern has a phase cone. In the olfactory bulb there appears to be only one phase cone at a time for the duration of the gamma burst. When there is more than one distinguishable component of the time-varying carrier frequency, each peak frequency has its phase cone with the same location and sign of the apex and the same phase velocity. The dual phase cones manifest the same broad-spectrum event. In neocortex there are multiple overlapping phase cones at all

times, giving the appearance of a pan of boiling water. The frequencies, signs and locations of the phase cones differ as much as they vary between successive events [21]. The distributions of the durations are power-law, and likewise of the diameters within the limits of measurement. The distributions of carrier frequencies and more generally of the power spectral densities in both time and space [21, 22, 27, 30] of neocortex are power-law. These multiple power-law distributions of the derived state variables suggest that neocortex is stabilized in a form of self-organized criticality (SOC) as first described by Bak, Wiesenfeld and Tang [4] and in more detail by Jensen [38].

The classic object of study of SOC is a sand pile fed from above as at the bottom of an hourglass. The steady drip of sand creates a conic pile that increases slope to a critical angle of repose that is held thereafter by repeated avalanches. Likewise a pan of water brought to a boil holds a constant temperature by forming bubbles of steam. An open system of interacting elements, whether grains of sand, water molecules or neurons, evolves to a stable steady state that is far from equilibrium. That global state is maintained at pseudo-equilibrium by repeated adjustments: avalanches of sand, bubbles of steam, or state transitions among groups of neurons. The records of the changes appear chaotic and give temporal and spatial spectra with $1/f^{\alpha}$ forms implying self-similarity across wide scales of time and space. Likewise the ECoG gives records that appear chaotic, with temporal and spatial power spectral densities that conform to $1/f^{\alpha}$, where the exponent α has been calculated as ranging $1 < \alpha < 3$ [20, 21, 22, 27, 51]. In all three systems the appearance of "noise" is illusory. When viewed from the proper perspective, informative structures in the "noise" become clear. The critical parameter that is maintained by SOC in cortex is proposed to be the mean firing rate of the neurons comprising the interactive populations in cortex, which is regulated homeostatically everywhere in cortex by the refractory periods. The mechanism is represented by a point attractor expressed in the pole at the origin of the complex plane (Figs. 6,7,8 and 9, right). Like avalanches the times and locations of cones are predictable not locally but only in the average. They overlap so that any neuron may participate in multiple cones simultaneously. The sizes and durations of cones give histograms that are power-law. The smallest and briefest cones are the most numerous. Their means and SD change in proportion to the size of the measuring windows [22, 30]. The distributions show that the neural patterns may be self-similar across multiple scales [12, 36, 37, 45, 51]. These functional similarities indicate that neocortical dynamics is scale-free [10, 19, 62]: the largest events are in the tail of a continuous distribution and share the same mechanism of onset and the same brief transit time of onset despite their large size.

6 A Proposed Phase Diagram to Represent the Dynamics of Cerebral Cortex

The classic phase diagram of a substance such as water at thermodynamic equilibrium (Fig. 12, A from Blauch [8]) serves as a platform from which to construct a diagram for cortex as a system operating far from equilibrium, yet maintaining a conditionally stable steady state (Fig. 12, B). The classic system is static and

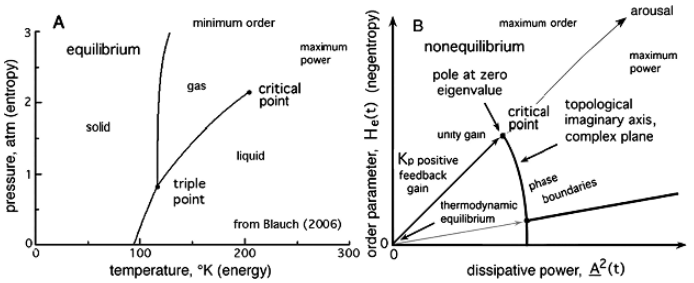

Fig. 12 (**A**) conventional phase diagram at equilibrium, from [8]. (**B**) by analogy to physical matter, a phase diagram is proposed for cortical dynamics. Far from equilibrium the levels of order and power are conceived to increase together with increased arousal (Fig. 1). The critical point and imaginary axis are taken from the complex plane (Fig. 9). Arousal from deep anesthesia (the "open loop" state with flat ECoG, KO in Fig. 4) leads to stabilization at a pseudo-equilibrium that is maintained by the refractory periods of the excitatory interactions among pyramidal (mitral) cells. Transformation of A to B is by translating the origin in B to the critical point shown in A and constructing two new orthogonal dimensions for change: the rate of pragmatic information increase (negentropy) as a scalar index of order on the ordinate and the rate of dissipation of free energy (power) on the abscissa

closed. The level of energy displayed on the abscissa is indexed by temperature. The degree of order displayed on the ordinate is measured by pressure, volume or entropy. Maximum order occurs at minimum energy. Three phases are separated by phase boundaries that meet at a triple point. However, the phase boundary between liquid and gas ends at a *critical point*, beyond which the phase of constituents is undefined.

Brains are open, dynamic systems that continually dissipate free energy [33, 60] in burning glucose; brains constitute 5% of body mass yet consume 20% of basal metabolic rate. Two new state variables are required: the rate of energy dissipation (power) on the abscissa, and the rate of increase in information (negentropy) on the abscissa, indexing the order emergent in dissipative structures [52]. In the dynamic display the equilibrium at criticality appears as a point at the origin of the new state variables. Equilibrium is approached in brain death and in the non-interactive state imposed by deep anesthesia (Fig. 4, KO). With recovery from anesthesia the degree of order and the rate of energy increase together (the diagonal line, Fig. 12, B).

Brain temperature is unsuitable as an index of power, because birds and mammals use homeostatic feedback to hold brain temperatures within a narrow range. A useful index of power is the mean square analytic amplitude, $\underline{A}^2(t)$, because ECoG amplitude depends on current density across the relatively fixed extracellular specific resistance of cortical tissue. The square of current or voltage is proportional to the power expended by neurons generating the dendritic potentials. This dissipation is the basis for imaging brain activity by measuring cerebral blood flow using fMRI, SPECT, PET, etc., because 95% of brain energy is consumed by oxidative metabolism in dendrites, only 5% in axons.

The degree of order on the ordinate is indexed by the scalar ratio specifying pragmatic information, $H_e(t)$. This state variable makes explicit the premise that order in dissipative structures increases with increasing power [52]. Cortex

indexCortexbreak operates as an open system far from equilibrium (Fig. 12, B), yet it is self-stabilized while transiting through a collection of states by processes variously denoted as orbiting in metastability [42, 57], chaotic itinerancy [40]; transient coherence in unitarily inequivalent ground states [33]; and bifurcations [35] among hierarchical levels by neuropercolation [Kozma Chapter] through an extension of random graph theory [42]. In all formulations the magnitude of the background activity at which the cortex is stabilized can vary; it generally co-varies with the level of arousal (Fig. 1). In cortex the stability is maintained by the refractory periods, so that no matter how great the increase in arousal, the output of the KIe populations is self-stabilized at unity feedback gain. The pole at the origin of the complex plane (Δ at the origin in Figs. 6,7,8 and 9) corresponds to the critical point (Δ) on the diagonally upward line (Fig. 12, B), so that the metastability of cortex can be described as an instance of self-organized criticality (SOC). Thereby the steady state can be described as a phase in a system at pseudo-equilibrium, and the state transition can be labeled as a phase transition. The demarcation by the imaginary axis that is accessible to piecewise linear analysis between stable and unstable states (Figs. 6,7,8 and 9) in the upper half of the complex plane is seen to correspond to a phase boundary (Fig. 12, B) between bistable receiving and transmitting states (Fig. 13). A second phase boundary that is inaccessible to linear analysis separates a phase domain of self-sustained complex partial seizure [16].

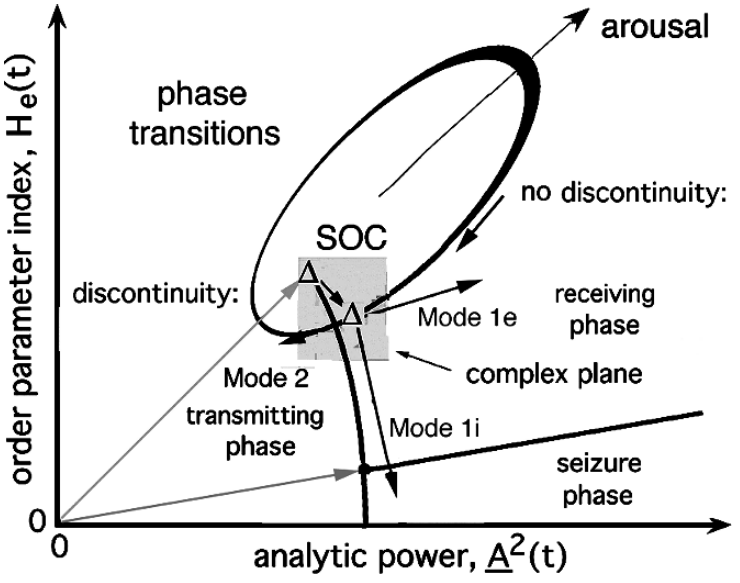

Fig. 13 A phase diagram of neocortical dynamics is constructed in the coordinates of the degree of order given by the rate of change in the order parameter, $H_e(t)$, as the dependent variable and the average analytic power, $\underline{A}^2(t)$, as the independent variable. The central grey area shows the linearized subspace of the complex plane in Figs. 6,7,8 and 9

These properties lead to a view of perception as a cyclical process (ellipse in Fig. 13). The cycle begins with cortex in a receiving state with an attractor landscape already established by learning from input and selected by the limbic system in preafference [39]. The pole at the origin representing the stable, non-zero point attractor of the KIe set (Δ at the origin in Figs. 6,7,8 and 9, right) specifies the location of the critical point (upper Δ) maintained by SOC, which is located on the 45° line that represents increasing order with increasing power of neural activity in accord with Prigogine's [52] "order from disorder" in formation of "dissipative structures" and Haken's [35] "slaving principle". Three phases are conceived in a simplified approach: receiving, transmitting, and seizure. The set point (Fig. 13, lower Δ) corresponding to the center small rectangle (unknown char) in Figs. 7,8 and 9 is postulated not to lie on the upwardly diagonal line but below the line. It is offset in sensory cortices by the background input from sensory receptors, and in other cortices by background input from other parts of the brain. The displacement (small downward arrow between triangles Δ — Δ in Fig. 13) reflects gain reduction below unity in for the smallest observable impulse responses (Fig. 6, A). The displacement represents decreased order and increased power.

The root locus in Mode 1e is represented by the nearly horizontal rightward arrow from the set point (lower Δ) indicating increased power and small increase in order with orthodromic evoked potentials above the range of background activity. The downward orange arrow indicates the root locus in Mode 1i, showing the increased power and decreased order accompanying impulse responses involving strong inhibition. The leftward magenta arrow indicates the root locus in Mode 2, which crosses the phase boundary (imaginary axis) in a phase transition. Mode 2 appears diametrically opposed to Mode 1e in showing a decrease in power with a small decrease in order, tending toward instability.

The most remarkable feature of the diagram in Fig. 13 is the description of the phase transition in an act of perception as *beginning with decreased power and decreased order*. This feature is counterintuitive, because perception is usually conceived as resulting from the impact of a sensory volley that increases power and imposes increased order by the injection of information from a stimulus. Certainly that takes place, but the phase diagram adds a different dimension to the story, as follows. The event that initiates a phase transition is an abrupt decrease in the analytic power of the background activity to near zero, as is shown to occur in Fig. 10, A, and as is simulated in B. This reduction induces a brief state of indeterminacy, in which the amplitude of the ECoG is near zero and phase of the ECoG is undefined. If a stimulus-induced volley arrives at or just before this state, then the cortex in accord with Mode 2 can be driven by the input across the phase boundary. The Mode 2 root loci in Fig. 9 show that exogenous input (as distinct from endogenous activity) increase amplitude and also instability by bringing the cortex closer and across the imaginary axis. The response amplitude depends not on the input amplitude but on the intrinsic state of the cortex, specifically the degree of reduction in the power and order of the background brown noise.

If the phase transition occurs, it re-sets the carrier frequency of oscillation through a discontinuity in analytic phase. Then the oscillation converges to a shared frequency (Fig. 9) as shown by the reduction in $SD_X(t)$ in Fig. 10, A. Thereafter

in succession follow re-synchronization as shown by increased $R_e(t)$ in Fig. 11, B; increased order as a stable pattern emerges with decreased $D_e(t)$ in Fig. 11, A; and lastly increased mean power $\underline{A}^2(t)$ in Fig. 11, A. After power has peaked, the cortex returns to its receiving state by a second phase transition without a discontinuity in the oscillatory phase. According to this hypothesis the cycle for the opportunity to undergo a phase transition repeats aperiodically at an intrinsic rate in the theta range. The actualization of a phase transition requires the presence of a surge of input to the cortex. In the experimental conditioning paradigm used in this study, the input surge is a sensory volley brought to the cortex by a behavioral act of observation, so the gamma ellipse in Fig. 13 can properly be called a representation of the neural trajectory of an action-perception cycle [17, 19, 28]. Conceivably the input surge can also be provided in sensory cortices by corticocortical transmission from the limbic system. Such a phase transition may underlie the formation of beta wave packets in a "virtual" action-perception cycle.

7 Conclusions and Summary

The significance of the reduction in power prior to initiation of a phase transition can be seen in the fact that an expected conditioned stimulus typically is a very weak signal that is embedded in contextual noise. The afferent volley activates the sensory cortex and actualizes the attractor landscape that expresses the several possible categories of CS that are expected during an intentional act of observation. A Hebbian nerve cell assembly that was formed in prior learning governs each attractor. The relatively few action potentials sent by the relevant receptors can ignite one of the cell assemblies, which can direct the cortex into the corresponding basin of attraction. That moment of selection can be conceived as done optimally when the background activity is quenched, and the output of a relevant Hebbian assembly has maximal signal:noise ratio in selecting a basin to which to guide the entire sensory cortex. When the background power then increases, it is imprinted with the AM pattern provided by an attractor in the landscape. The power is not provided by the sensory input; it is provided by the intrinsic mutual excitation. The null spike may be likened to the eye of a hurricane—a transient interlude of silence that opens the possibility for a change in direction of movement. The next null spike quenches the cortical activity and releases the dynamics from the attractor as the AM pattern disappears.

The null spike in the band pass filtered brown noise activity is conceived as a *shutter* [43] that blanks the intrinsic background. At very low analytic amplitude when the analytic phase is undefined, it may be that the system trajectory approaches a singularity that enhances the likelihood for a small extrinsic sensory input to re-set the background activity in a new frame. The null spike does not qualify as a gate, because the sensory input is not blocked or withheld, and the AM pattern in the following frame, if any, is formed by reorganization of existing activity through attractor selection, not by the driving of cortical activity by input as in the "information processing" model. The null spike is not a scanner [61], because the

selection of a basin of attraction is by competition among cell assemblies in state space and not by a search for a module in cortex. It is not really a clock, because the recurrence of null spikes is aperiodic in a limited range, and the formation of an AM pattern requires an exogenous factor, the input as from a sniff or a saccade [58]. Gating, scanning, and clock timing [46] are better conceived as mesoscopic thalamocortical operations Bressler Chapter], while the precise timing of the phase transition is performed within the neural populations that are to construct the wave packet carrying an AM pattern. Exploration will require development of a mathematical foundation for the null spike, which does not currently exist. Two promising bases for research are foreseen in random graph theory [9, 42] and quantum field theory [33, 60]. They are approaches widely used to describe processes by which microscopic events might be up-scaled into macroscopic patterns in complex systems.

Figure 13 offers the basis for more complicated graph in which to synthesize and display further data and concepts derived from studies of the nonlinear dynamics of cortex. This simple form can be elaborated to include additional data from drug studies. For example, induction of anesthesia by barbiturates is by enhancement of inhibition that is replicated by the root locus in Mode 1i. The same root loci are obtained by reducing the background activity with barbiturate or by increasing the impulse intensity (Fig. 8). At the extreme level of flattening the ECoG, the gain $k_p = 0$, and a point attractor with zero amplitude is revealed [32] giving the open loop impulse response (Fig. 4, KO). An instability is manifested in barbiturate spindles: brief bursts of oscillation in the theta range [14]. Stages of sleep might be represented by yet other phases.

Brief tetanization of the lateral olfactory tract at supra-maximal intensity can induce a complex partial seizure with *absence* and 3/s spike-and-wave [16]. This autonomous pattern of activity implies the existence of the lower phase boundary that separates the receiving and transmitting states from an epileptic domain with very high power and minimal order, which is accessed paradoxically by raising the activity of mutually inhibitory neurons to high intensity. Remarkably the seizure spike repetition rate is also in the same theta range as the null spike. The seizure spike-and-wave would form a much larger ellipse (not shown).

The normal ellipse might be regarded as a 2-D projection of a torus, which manifests a quasi-periodic attractor, in which the low frequency of burst repetition in the theta range is represented by the diameter of the torus, and the high frequency of the burst carrier wave in the beta or gamma range is represented by the thickness of the torus. The torus might in turn be regarded as a projection of a helix extending into the time domain in 3-D. Multiple ellipses might serve to represent high-dimensional chaotic attractor landscapes [32], dynamic memory systems in neuropercolation theory [56], and multiple ground states modeled by dissipative quantum field theory [16, 60]. More immediately, a solid mathematical foundation is needed beyond ODE, in order to derive and describe more precisely the forms of the neural action-perception cycles and the phase boundaries that they cross, for which ODE are not fully suitable.

In summary, the olfactory bulb, nucleus and cortex constitute a semi-autonomous system in each cerebral hemisphere that receives odorant information, categorizes

an odor percept by generalization and abstraction, and transmits the percept broadly through the forebrain. The form of the percept is a frame constructed and carried by a wave packet with an aperiodic "chaotic" carrier oscillation in the gamma range. The content is expressed in a spatial pattern of amplitude modulation (AM) of the carrier wave that is determined by modified synapses among bulbar mitral cells that form Hebbian nerve cell assemblies in reinforcement learning. Each cell assembly for a discriminated odorant guides the bulb to an AM pattern constructed by a "chaotic" attractor. The collection of learned categories of odors is retained in the form of an attractor landscape. Each attractor is surrounded by a basin of attraction; the processes of generalization and abstraction occur when the system converges to the attractor, regardless of where in a basin a stimulus places the system. Three requirements met by the olfactory system in percept formation are a state transition from a receiving state to a transmitting state, another to return, and a third for repeated sampling of the olfactory environment: a shutter.

Dynamics in the visual, auditory and somatic perceptual systems share these properties. In this Chapter evidence from ECoG of allocortex and neocortex serves to describe the neural mechanisms that generate and stabilize cortical carrier waves; that enable the state transitions; and that provide a shutter to terminate old frames and initiate new ones in cinematographic sequences in every sensory system. It is postulated that a percept forms a wave packet only when the endogenous background activity briefly abates in a "null spike", which provides the high signal:noise ratio that a burst of cortical activity that is driven by input relayed from sensory receptors needs to select and initiate a new frame. The aperiodic sequence of null spikes provides the shutter that is a necessary though not sufficient condition for the cinematographic process of perception.

Acknowledgment I am grateful to Mark D. Holmes and Ceon Ramon, University of Washington, Seattle WA and Sampsa Vanhatalo, University of Helsinki, Finland for data and modeling using 64 channels of the 256-channel recording System 200 provided by Don Tucker, Electrical Geodesics Inc., Eugene OR. For critical insights I am grateful to physicists Giuseppe Vitiello, Salerno University and Michael Stringer, Northwestern University, and to mathematicians Robert Kozma, Memphis University and Béla Bollobás, Cambridge University. A preliminary version of this Chapter appears in Proc. IJCNN'07 [23].

References

1. *Neurodynamics. An Exploration of Mesoscopic Brain Dynamics*. London: Springer, 2001.
2. D. J. Amit. The hebbian paradigm reintegrated: Local reverberations as internal representations. *Behavioral and Brain Science*, 18:617–657, 1995.
3. H. Atmanspacher and H. Scheingraber. Pragmatic information and dynamical instabilities in a multimode continuous-wave dye laser. *Canadian Journal of Physics*, 68:728–737, 1990.
4. P. Bak, C. Tang C, and K. Wiesenfeld. Self-organized criticality: an explanation of 1/f noise. *Physical Review Letters*, 59:364–374, 1987.
5. J. M. Barrie, W. J. Freeman, and M. Lenhart. Modulation by discriminative training of spatial patterns of gamma eeg amplitude and phase in neocortex of rabbits. *Journal of Neurophysiology*, 76:520–539, 1996.

6. E. Basar. Eeg - brain dynamics. *Amsterdam: Elsevier*, 1980.
7. E. Basar. Brain function and oscillations. *Berlin: Springer-Verlag*, 1998.
8. D. N. Blauch. Chemistry experiments & exercises: Phase changes. 2006.
9. B. Bollobás. Random graphs, cambridge studies in advanced mathematics 2nd ed. *Cambridge UK: Cambridge University Press*, 1985/2001.
10. B. Bollobás and O. Riordan. *Results on scale-free random graphs*. Weinhiem: Wiley-VCH, 2003.
11. S. L. Bressler and J. A. S. Kelso. Cortical coordination dynamics and cognition. *Trends in Cognitive Science*, 5:26–36, 2001.
12. C. L. Chapman, P. D. Bourke, and J. J. Wright. Spatial eigenmodes and synchronous oscillation: coincidence detection in simulated cerebral cortex. *Journal of Mathematical Biology*, 45:57–78,, 2005.
13. J. D. Emery and W. J. Freeman. Pattern analysis of cortical evoked potential parameters during attention changes. *Physiololgy and Behavior*, 4:67–77, 1969.
14. W. J. Freeman. Mass action in the nervous system. *New York: Academic Press*, 1975.
15. W. J. Freeman. Nonlinear gain mediating cortical stimulus-response relations. *Biological Cybernetics*, 33:237–247, 1979.
16. W. J. Freeman. Petit mal seizure spikes in olfactory bulb and cortex caused by runaway inhibition after exhaustion of excitation. *Brain Research Reviews*, 11:259–284, 1986.
17. W. J. Freeman. *Societies of Brains. A Study in the Neuroscience of Love and Hate*. Mahwah NJ: Lawrence Erlbaum Assoc., 1995.
18. W. J. Freeman. Origin, structure, and role of background eeg activity. part 3. neural frame classification. *Clinical. Neurophysiology*, 116(5):1118–1129, 2005.
19. W. J. Freeman. Definitions of state variables and state space for brain-computer interface. part 1. multiple hierarchical levels of brain function. *Cognitive Neurodynamics*, 1(1): 3–14, 2006.
20. W. J. Freeman. Origin, structure, and role of background eeg activity. part 1. phase. *Clinical. Neurophysiology*, 115:2077–2088, 2006.
21. W. J. Freeman. Origin, structure, and role of background eeg activity. part 2. amplitude. *Clinical. Neurophysiology*, 115:2089–2107, 2006.
22. W. J. Freeman. Origin, structure, and role of background eeg activity. part 4. neural frame simulation. *Clinical. Neurophysiology*, 117(3):572–589, 2006.
23. W. J. Freeman. Cortical aperiodic 'clock' enabling phase transitions at theta rates. *Proceedings, International Joint Conference on Neural Networks (IJCNN)*, 2007.
24. W. J. Freeman and B. Baird. Relation of olfactory eeg to behavior: Spatial analysis. *Behavioral Neuroscience*, 101:393–408, 1987.
25. W. J. Freeman and B. C. Burke. A neurobiological theory of meaning in perception. part 4. multicortical patterns of amplitude modulation in gamma egg. *International Journal of Bifurcation and Chaos*, 13:2857–2866, 2003.
26. W. J. Freeman, B. C. Burke, and M. D. Holmes. Aperiodic phase re-setting in scalp eeg of beta-gamma oscillations by state transitions at alpha-theta rates. *Human Brain Mapping*, 19(4):248–272, 2003.
27. W. J. Freeman, B. C. Burke, M. D. Holmes, and S. Vanhatalo. Spatial spectra of scalp eeg and emg from awake humans. *Clinical. Neurophysiology*, 114:1055–1060, 2003.
28. W. J. Freeman, G. Gaál, and R. Jornten. A neurobiological theory of meaning in perception. part 3. multiple cortical areas synchronize without loss of local autonomy. *International Journal of Bifurcation and Chaos*, 13:2845–2856, 2003.
29. W. J. Freeman and K. Grajski. Relation of olfactory eeg to behavior: Factor analysis. *Behavioral Neuroscience*, 100:753–763, 1987.
30. W. J. Freeman, M. D. Holmes, G. A. West GA, and S. Vanhatalo. Fine spatiotemporal structure of phase in human intracranial egg. *Clinical Neurophysiology*, 117: 1228–1243, 2006.
31. W. J. Freeman and L. J. Rogers. A neurobiological theory of meaning in perception. part 5. multicortical patterns of phase modulation in gamma eeg. *International Journal of Bifurcation and Chaos*, 13:2867–2887, 2003.

32. W. J. Freeman and W. Schneider. Changes in spatial patterns of rabbit olfactory eeg with conditioning to odors. *Psychophysiology*, 19:44–56, 1982.
33. W. J. Freeman and G. Vitiello. Nonlinear brain dynamics as macroscopic manifestation of underlying many-body field dynamics. *Physics of Life Reviews*, 3:93–118, 2006.
34. E. Gordon. Integrative neuroscience. *Sydney: Harwood Academic*, 2000.
35. H. Haken. *What can synergetics contribute to the understanding of brain functioning?* C. Uhl (Ed.) Berlin: Springer-Verlag, 1999.
36. R. C. Hwa and T. Ferree. Scaling properties of fluctuations in the human electroencephalogram. *Physics Review*, 66, 2002.
37. L. Ingber. Statistical mechanics of multiple scales of neocortical interactions. *Nunez PL (ed.) Neocortical Dynamics and Human EEG Rhythms, New York: Oxford University Press*, pp. 628–681, 1995.
38. H. J. Jensen. Self-organized criticality: Emergent complex behavior in physical and biological systems. *New York: Cambridge University Press*, 1998.
39. L. M. Kay and W. J. Freeman. Bidirectional processing in the olfactory-limbic axis during olfactory behavior. *Behavioral Neuroscience*, 112:541–553, 1998.
40. J. A. S. Kelso. Dynamic patterns: The self-organization of brain and behavior. *Cambridge: MIT Press*, 1995.
41. R. Kozma and W. J. Freeman. Chaotic resonance: Methods and applications for robust classification of noisy and variable patterns. *International Journal of Bifurcation and Chaos*, 10:2307–2322, 2001.
42. R. Kozma, M. Puljic, P. Balister, B. Bollobás, and W. J. Freeman. Phase transitions in the neuropercolation model of neural populations with mixed local and non-local interactions. *Biological Cybernetics*, 92:367–379, 2005.
43. K. S. Lashley. *Brain Mechanisms and Intelligence*. Chicago IL: University of Chicago Press, 1929.
44. D. T. J. Liley, M. P. Dafilis, and P. J. Cadusch. A spatially continuous mean field of electrocortical activity. *Network: Computational Neural Systems*, 13:67–113, 2002.
45. K. Linkenkaer-Hansen, V. M. Nikouline, J. M. Palva, and R. J. Iimoniemi. Long-range temporal correlations and scaling behavior in human brain oscillations. *Journal of Neuroscience*, 15:1370–1377, 2001.
46. M. S. Matell and W. H. Meck. Neuropsychological mechanisms of interval timing behavior. *BioEssays*, 22(1):94–103, 2000.
47. M. Merleau-Ponty. Phenomenology of perception. *New York: Humanities Press*, 1945/1962.
48. F. W. Ohl, H. Scheich, and W. J. Freeman. Change in pattern of ongoing cortical activity with auditory category learning. *Nature*, 412:733–736, 2001.
49. J. Orbach. The neuropsychological theories of lashley and hebb. *Psycoloquy*, 10(29), 1999.
50. J. Panksepp. Affective neuroscience: The foundations of human and animal emotions. *Oxford UK: Oxford University Press*, 1998.
51. E. Pereda, A. Gamundi, R. Rial, and J. Gonzalez. Non-linear behavior of human eeg – fractal exponent versus correlation dimension in awake and sleep stages. *Neuroscence Letters*, 250:91–94, 1998.
52. I. Prigogine. From being to becoming: Time and complexity in the physical sciences. *San Francisco. W. H. Freeman*, 1980.
53. G. Viana Di Prisco and W. J. Freeman. Odor-related bulbar eeg spatial pattern analysis during appetitive conditioning in rabbits. *Behavioral Neuroscience*, (99):962–978, 1985.
54. O. Sacks. In the river of consciousness. *New York Book Revue*, 51(1), 2004.
55. M. Schroeder. Fractals, chaos, power laws. *San Francisco: W. H. Freeman*, 1991.
56. L. Siklós, M. Rickmann, F. Joó, W. J. Freeman, and J. R. Wolff JR. Chloride is preferentially accumulated in a subpopulation of dendrites and periglomerular cells of the main olfactory bulb in adult rats. *Neuroscience*, 64:165–172, 1995.
57. C. A. Skarda and W. J. Freeman. How brains make chaos in order to make sense of the world. *Behavioral and Brain Science*, 10:161–195, 1987.
58. L. W. Stark, C. M. Privitera, H. Yang, M. Azzariti, Y. F. Ho, T. Blackmon, and D. Chernyak. Representation of human vision in the brain: How does human perception recognize images? *Journal of Electronic Imaging*, 10(1):123–151, 2001.

59. I. Tsuda. Towards an interpretation of dynamic neural activity in terms of chaotic dynamical systems. *Behavioral and Brain Sciences*, 24:793–810, 2001.
60. G. Vitiello. My double unveiled. *Amsterdam: John Benjamins*, 2001.
61. W. G. Walter. *The Living Brain*. New York: W. W. Norton, 1953.
62. X. F. Wang and G. R. Chen. Complex networks: small-world, scale-free and beyond. *EEE Circuits and Systems*, 31:6–20, 2003.
63. J. J. Wright, C. J. Rennie, G. J. Lees, P. A. Robinson, P. D. Bourke, C. L. Chapman, E. Gordon, and D. L. Rowe. Simulated electrocortical activity at microscopic, mesoscopic and global scales. *Journal of Neuropsychopharmacology*, 28:S80–S93, 2003.